Synthesis and application of triphenylamine-based aldehydes as photo-initiators for multi-photon lithography

D. Ladika, G. Noirbent, F. Dumur, D. Gigmes, A. Mourka, G. Barmparis, M. Farsari, D. Gray

Synthesis and application of triphenylamine-based aldehydes as photo-initiators for multi-photon lithography

D. Ladika[1,2], G. Noirbent[3], F. Dumur[3], D. Gigmes[3], A. Mourka[4*], M. G. D. Barmparis[5], M. Farsari[1], and D. Gray[1*]

[1] Institute of Electronic Structure and Laser, Foundation for Research and Technology-Hellas, 70013 Heraklion, Crete, Greece
[2] Department of Materials Science and Technology, University of Crete, 70013 Heraklion, Crete, Greece
[3] Aix Marseille Univ, CNRS, ICR, UMR 7273, F-13397 Marseille, France
[4] Department of Electrical and Computer Engineering, Hellenic Mediterranean University, Heraklion, Greece
[5] Department of Chemistry, University of Crete, 70013 Heraklion, Crete, Greece

*amourka@iesl.forth.gr
*dgray@iesl.forth.gr
Received xxxxxx
Accepted for publication xxxxxx
Published xxxxxx

Abstract

Photopolymerization of (meth)acrylate-based formulations has become a widespread method for industry due to the high energy efficiency and low curing times of this technology. Various products from simple coatings to more complex applications such as additive manufacturing technologies are based on this versatile method. Common industrial radical photoinitiators are generally based on aromatic ketones. Benzaldehyde is an organic compound consisting of a benzene ring with a formyl substituent. It is the simplest aromatic aldehyde and one of the most industrially useful; for instance in the preparation of various aniline dyes, perfumes, flavorings, and pharmaceutics. Parallel to this, triphenylamines are extensively used for the design of dyes used for solar energy conversion. In this work, three triphenylamine derivatives bearing formyl groups are as a new substance class of multi-photon lithography photoinitiators. Besides their efficient formulations, they show high biocompatibilty by investigating the adhesion, viability and proliferation of dental stem cells on photopolymerized thin films.

Keywords: multiphoton polymerization, non-linear lithography, micro/nano additive manufacturing, biocompatibility, cell culture, tissue engineering, triphenylamine

1. Introduction

Multi-photon Lithography (MPL) is a laser-based direct-writing technique for the fabrication of 3D structures in microscale with submicron resolution via a computer-aided design (CAD) [1, 2]. The demand for more complex 3D microstructures in order to be applied in areas like tissue engineering [3], single cell studied metamaterials [4] and nanophotonic structures [5],was the driving force for MPL to be utilised [6]. MPL technique is based on the phenomenon of Multiphoton Absorption (MPA) that Goeppert-Mayer and coworker first reported in 1931, which adresses the simultaneous absorption of two or more photons [7].

In MPL, a femtosecond laser beam is tightly focused into a small volume of a photosensitive material. Due to the nonlinearity between the multiphoton excitation of the PI and the intensity of the laser source, the polymerization is confined to a small, well-defined volume, so called voxel, within the laser beam focus, where the intensity is high enough for the PI to initiate the polymerization [8]. During the polymerization, the monomers are converted into a robust polymer network. This additive manufactuirng technique is based on radical polymerization mechanism, which requires the use of a

photosensitive molecule, called photoinitiator (PI), apart from the monomer, to initiate the polymerization by the production of free radicals, following the multiphoton absorption [9]. The synthesis of novel polymers and high-performance PIs for MPL have been the subject of investigation during the last years; enabling true 3D printing within a monomer formulation featuring excellent spatial control and taking advantgae of well-defined penetration depths by the use of a long wavelength excitation source (typically ≈ 800nm) [10,11]. While the size of the activated voxel can be below the diffraction limit positions outside of this volume are not affected. Consequently, this polymerization technique offers high resolution while minimizing unwanted thermal or photochemical initiation of UV-photoinitiators [12].
…… radical polymerization…
…… commonly used photinitiators…
…… why the tested materials here are of interest…

2. Experimental

2.1 Materials

All solvents were purchased from Sigma-Aldrich (Steinheim, Germany) and were used without further purification. Methacryloxypropyl trimethoxysilane (MAPTMS, 97%), 2-(dimethylamino) ethyl methacrylate (DMAEMA, 98%), zirconium *n*-propoxide (ZPO, 70% in propanol), 4,4-*bis*(diethylamino)benzophenone (BIS, >99%), ascorbic acid, phalloidin-Atto 488, 4′,6-diamidino-2-phenylindole (DAPI) and Alizarin Red S were purchased from Sigma-Aldrich (Steinheim, Germany). Cell culture medium, (alpha-MEM), fetal bovine serum (FBS), antibiotic/antimycotic, glutamine and the PrestoBlue® reagent were purchased from Invitrogen (Karlsruhe, Germany) and Triton X-100 from Merck (Darmstadt, Germany).

2.2 Photoinitiators synthesis

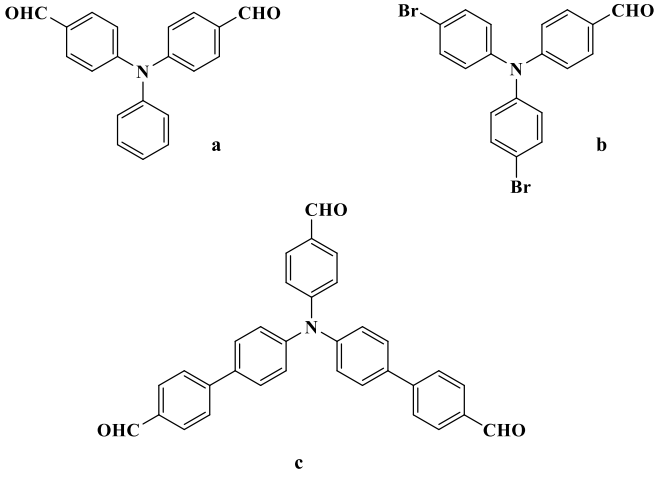

Figure 1. Molecular structure of photoinitiators discussed in this work.

All reagents and solvents were purchased from Aldrich or Alfa Aesar and used as received without further purification. Mass spectroscopy was performed by the Spectropole of Aix-Marseille University. ESI mass spectral analyses were recorded with a 3200 QTRAP (Applied Biosystems SCIEX) mass spectrometer. The HRMS mass spectral analysis was performed with a QStar Elite (Applied Biosystems SCIEX) mass spectrometer. Elemental analyses were recorded with a Thermo Finnigan EA 1112 elemental analysis apparatus driven by the Eager 300 software. ^{1}H and ^{13}C NMR spectra were determined at room temperature in 5 mm o.d. tubes on a Bruker Avance 400 spectrometer of the Spectropole: ^{1}H (400 MHz) and ^{13}C (100 MHz). The ^{1}H chemical shifts were referenced to the solvent peak $CDCl_3$ (7.26 ppm) and the ^{13}C chemical shifts were referenced to the solvent peak $CDCl_3$ (77.0 ppm). Compounds a [RSC Adv., 2016, 6, 8628–8638] and b [J. Am. Chem. Soc. 2019, 141, 14565−14569] have been prepared according to procedures reported in the literature, without modification and in similar yields.

Synthesis of 4',4'''-((4-formylphenyl)azanediyl)bis(([1,1'-biphenyl]-4-carbaldehyde)) ***c***

Tetra*kis*(triphenylphosphine)palladium (0) (0.46 g, 0.744 mmol, M = 1155.56 g.mol^{-1}) was added to a mixture of 4-(*bis*(4-bromophenyl)amino)benzaldehyde (2.52 g, 6.11 mmol, M = 413.13 g.mol^{-1}), (4-formylphenyl)boronic acid (1.90 g, 12.66 mmol, M = 149.94 g.mol^{-1}), toluene (54 mL), ethanol (26 mL) and an aqueous potassium carbonate solution (2 M, 6.91 g in 25 mL water, 26 mL) under vigorous stirring. The mixture was stirred at 80 °C for 48 h under a nitrogen atmosphere. After cooling to room temperature, the reaction mixture was poured into water and extracted with ethyl acetate. The organic layer was washed with brine several times, and the solvent was then evaporated. Addition of dichloromethane followed by pentane precipitated a white solid which was filtered off. The residue was purified by column chromatography (SiO_2, gradient of solvents from pentane/ dichloromethane: 1/1 and pure dichloromethane) enabling to isolate the targeted compound as a solid (2.5 g, 85% yield). ^{1}H NMR (400 MHz, $CDCl_3$) δ: 7.19 (d, 2H, J = 8.6 Hz), 7.29 (d, 4H, J = 8.6 Hz), 7.65 (d, 4H, J = 8.6 Hz), 7.77 (dd, 6H, J = 8.7 Hz, J = 2.2 Hz), 7.97 (d, 4H, J = 8.4 Hz), 9.98 (s, 1H), 10.06 (s, 2H); ^{13}C NMR (100 MHz, $CDCl_3$) δ: 121.2, 126.1, 127.3, 128.7, 130.4, 131.4, 135.2, 136.1, 146.0, 146.5, 152.6, 190.4, 191.7; HRMS (ESI MS) m/z: theor: 482.1751 found: 482.1745 ($[M+H]^+$ detected).

2.5 Photopolymer synthesis

The photopolymer in use is an organic-inorganic composite and was developed through Sol-Gel process like SZ2080 in referenc, but instead of Methacrylic Acid (MAA), we mixed 2-(Dimethylamino) ethyl methacrylate (DMAEMA) [13]. In this application, it benefits from the dimensional accuracy and lack of shrinkage of this zirconium/silicon hybrid material, as well as its biocompatibility. The hybrid photoresist is composed of [3-(Methacryloyloxy) propyl] trimethoxysilane (MAPTMS), (DMAEMA) and Zirconium *n*-propoxide (ZPO, 70% in propanol). Regarding the photoresist's synthesis, hydrolysis of MAPTMS using HCL solution (0.1M) at a ratio

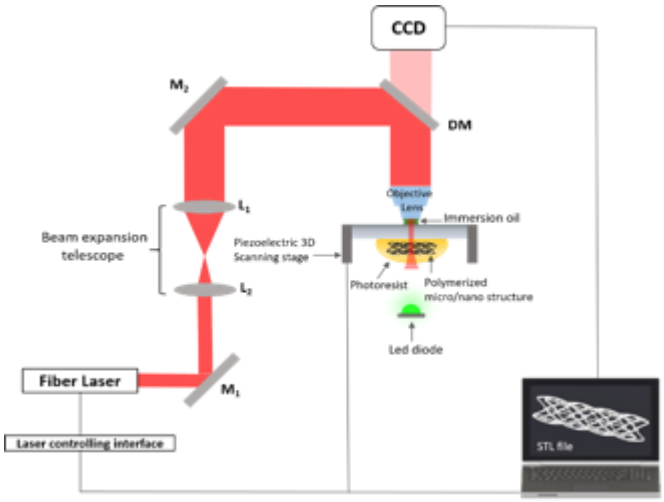

of 1:0.1 occurred, while ZPO and MAPTMS were mixed in order to form the inorganic network. The ratios of the chemical components are the following: MAPTMS: ZPO=8:2 and (MAPTMS+ZPO): DMAEMA=3:1. The three tested photoinitiators (Figure 1) in this work and the molecule 4,4′-*bis*(diethylamino)benzophenone (BIS), which is one of the standard photoinitiators in MPL, were dissolved in dichloromethane (DCM) and 1-propanol, respectively. Then, they were mixed at 1% w/w concentration in the final solution of MAPTMS and DMAEMA. The photopolymer was filtered via a 0.22μm syringe filter prior use and storage.

2.6 UV-Vis Absorption Spectroscopy

The Perkin Elmer, model Lambda 25, UV−vis spectrophotometer was employed to record the UV−vis absorption spectra of the samples. The measurements were fulfilled from 300nm to 800nm. The PIs were dissolved in dichloromethane to a concentration 1:100 and placed quartz cuvettes. The results are compared to *4,4' Bis (diethylamino) benzophenone* that was dissolved in 1-propanol, to the same concentration (Figure 2a). A fundamental condition for an efficient PI, is to be transparent at the employed laser wavelength (i.e. 780nm), allowing the transmission of the incident laser beam and in-volume (voxel) focusing. Moreover, an efficient PI should be transparent at the two-photon absorption wavelength (λ/2) to avoid thermal damage or ablation, which is applied for the discussed PIs since their absorption peak is at 375nm [14]. Regarding the photoluminescence (PL) spectra, a blue shift is recorded for the discussed PIs compared to Bis, as the luminescence peak for Bis is centered at 550 nm and for the other three tested PIs is at ~460nm (Figure2b).

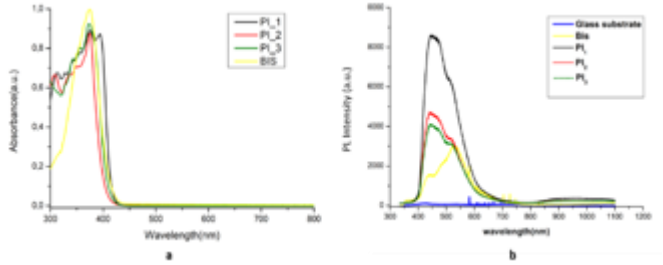

Figure 2. **a.** UV-visible *absorption spectra of the three tested PIs in dichloromethane and the standard PI (Bis) in 1-Propanol.* **b.** *Photoluminescence emission spectra at room temperature using a 248nm KrF laser as excitation source.*

2.7 Sample Preparation

The glass substrates (coverslips) in use were cleaned by sonication in acetone for 1 hour, followed by rinsing with methanol for 30 min. To enhance the adhesion of the fabricated 3D structures onto the substrates, the latter were steeped with MAPTMS (monomer). Then, the thin (120μm) flat glass substrates (with 13mm diameter) were placed in a dichloromethane/MAPTMS solution (1:250 v/v) under sonication for 4 hours, followed by rinsing with ethanol several times and drying under a nitrogen gas stream. The samples were prepared through photopolymer drop casting onto the flat glass substrates, while the resultant drops were dried in vacuum at room temperature for 24 hours, before photopolymerization.

For thin film preparation, 40 μL of the tested photopolymer were spin-coated at 4000 rpm for 60 seconds. Next, the organic vinyl bonds of the photopolymer in use were photopolymerized using a UV lamp at 365 nm to form a hybrid double network. Finally, the polymerized films were developed for 1 hour in 4-methyl-2-pentanone and dried at 100 °C for 30 min.

2.8 Experimental Setup

We tested three benzaldehyde moieties as a new substance class of multi-photon polymerization using a custom-designed MPL setup, based on a femtosecond laser guided into a stage scanning microfabrication work station. The expanded and collimated femtosecond laser beam is guided through the microscope objective (oil-immersion lens, 100x, N.A. = 1.4, Zeiss, Plan Apochromat and 40x, N.A.=0.95, Zeiss, Plan Apochromat) focusing it into the volume of the tested photopolymer. The photopolymers under this study are transparent to VIS or near IR wavelengths, so one can target the vicinity of the focused beam deep into the bulk (the depth is limited only by the working distance of the microscope objective). The sample is mounted on XYZ translation stage (Physik Instrumente M- 110.1DG) that ensures an overall travelling of 150um into X and Y directions and 50um in Z direction with high accuracy (50nm minimum incremental motion).

Figure 3. MPP fabrication setup. Laser power is controlled with attenuator which consitsts of a polarizer and a λ/2 plate. Femtosecond laser beam is guided through optical system, reflected by dichroic mirror and coupled to objective lens. Sample is fixed on XYZ stage which is computer controlled. LED provides illumination needed for CCD to monitor the fabrication process online. M: mirror, L: lens, DM: dichroic mirror, CCD: charged-coupled device.

Upon irradiation, the pre-polymer undergoes transition from liquid state to solid state (or from gel to solid) and this results in the change of refractive index. It enables wide-field

transmission or reflection microscopy (depending on whether the sample is transparent or opaque) to be used for monitoring of the manufacturing process in real time.

A microscope is built by adding to the system a source of green LDE, a CCD and a video screen. It is of utmost importance to anchor the microstructures to the substrates for them to survive the development (washing) steps of the unsolidified photopolymer. By moving the sample three-dimensionally inside the photopolymer in use, the position of laser focus is changed and one is able to write complex 3D structures (Figure 3). 3D micro-structures can be imported from CAD files or programmed directly.

2.9 Cell viability and proliferation assay

A suspension of 3 × 104 cells in α-MEM was seeded on the specimens with film coatings of the hybrid material (30%DMAEMA and PIs) and was placed into the cell culture incubator at 37 °C. On days 2, 4, and 7 post seeding, the cell viability and proliferation assays were performed with the reassuring-based PrestoBlue reagent according to the manufacturer's instructions. The reagent was incubated on the cells at 37 °C for 60 min. The absorbance was measured by a spectrophotometer (Synergy HTX Multi-Mode Microplate Reader, BioTek, Winooski, VT), and the cell number quantification was performed by means of a calibration curve. Error bars representing the average of triplicates ± standard deviation in two independent experiments were calculated (n = 6). Additionally, the cells on the polymerized thin films were examined daily for 7 days and visualized by optical microscopy by means of a Zeiss Axiovert 200 microscope. Images were taken by a ProgResVR CFscan Jenoptik camera (Jena, Germany) using ProgResVR CapturePro 2.0 software and objective lenses for 10-fold magnification.

2.10 Statistical analysis

Statistical analysis was performed using the one-way analysis of variance Dunnett's multiple comparisons test. To statistically evaluate the difference in cell proliferation after certain time points (2, 4, and 7 days), we compared the hybrid material films at each time point against the control tissue culture polystyrene (TCPS) surface. Statistical significance was set for $p < 0.05$.

3. Results and discussion

3.1 Investigating the order of non-linearity of the photoresist

In a recent study done by Mueller et al [15], the effective non-linearity of different photoresists was determined by varying the repetition rate, $\boldsymbol{R}$, of the electronically pulsed laser diode and following a scheme similar to [16]. The exposure dose was expressed as $\boldsymbol{D \propto R \cdot \Delta t \cdot I_p^q}$, where $\boldsymbol{\Delta t}$ is the pulse length and $\boldsymbol{I_p}$ is the peak intensity of the pulses. Then, the threshold peak power, which is proportional to the threshold pulse peak intensity, becomes, $\boldsymbol{P_{th} \propto (R \cdot \Delta t)^{-\frac{1}{q}}}$. Thus, the non-linearity could be measured directly by varying $\boldsymbol{R}$ or $\boldsymbol{\Delta t}$ and determining the respective threshold laser power. Upon the same principle, the threshold laser power – scanning speed relation can be generalized for a q-photon process as $\boldsymbol{P_{th} = c \cdot \sqrt[q]{V}}$, where c is a constant and V is the scanning speed. Hence, by identifying the power threshold for a given scanning speed, one can calculate through a linear regression on the data analysis the remaining two parameters. We obtained as shown in Figure 4, separated lines with length 10μm for every scanning speed while varying the laser power from 1 to 15 mW, in 1 mW steps. Furthermore, we set the

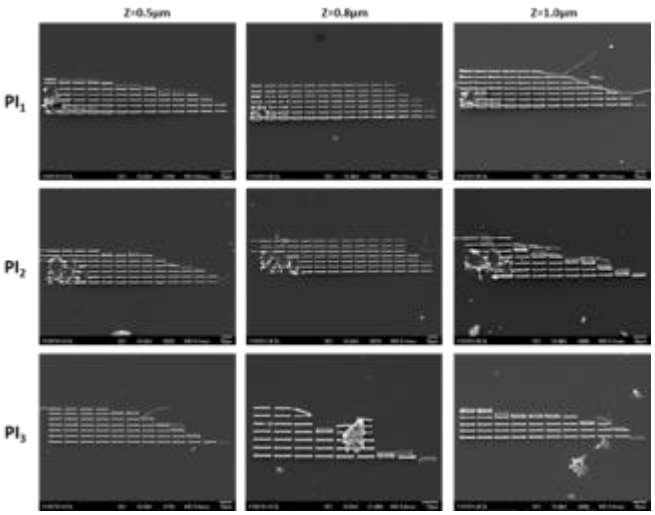

location of the focused laser beam between 0.5-1.0μm (upper from the surface of a glass substrate) for subsequent verification. The patterns consist of lines with increasing laser power (from under-exposed, through normal exposure, up to the damage threshold) and different z-positions (from focusing into the glass volume to writing within the resist volume without contact to the surface).

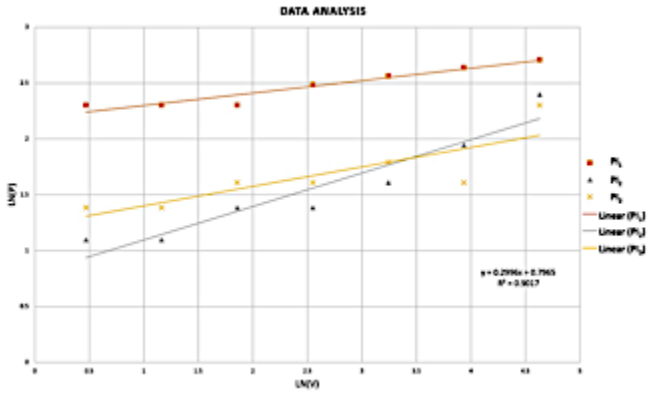

Figure 4. Experimentally determined polymerization thresholds for the photoresists discussed in this work and threshold laser power vs. the writing scanning speed (for z=0.8um). Seven spots are actual data collected for the tested scanning speeds and lines are linear fits according to the Eq. (2).

Laser power is an important cue to obtain desired features. If laser power is too low or too high, photoresists cannot be polymerized or burns off, respectively. In this manner, one can identify the process window of the tested materials as we discuss next.

The polymerization threshold is defined as the lowest laser power that yields well defined polymer lines after the development process. We can determine the polymerization threshold *in situ*, as it is observed on the video camera during the writing process. Additionally, the damage threshold can be judged by the visible occurrence of micro-explosions that appear as opaque bubbles.

The resulting polymerization-threshold laser powers are depicted in *Figure 4* as point spots. As expected, the laser powers needed for polymerization increase with increasing the scanning speeds. Within this simple threshold model, we can predict the scaling of the polymerization-threshold laser power. The threshold laser power needed to induce a *q*-photon-absorption process while scanning with a velocity, *V*, is given by

$$P_{th,i} = c \cdot \sqrt[q]{V_i} \quad (1)$$

where *c* is a constant and *q* the order of the non-linear process. Solving this equation by taking the natural logarithmic function (*ln*) of both sides, results in

$$ln\left(P_{th,i}\right) = ln(c) + \frac{1}{q} ln(V_i) \quad (2)$$

Thus, by applying a linear regression on the data analysis, for instance for the first tested photoresists (PI_1); a linear fit corresponds to a straight line:

$$y = 0.2996x + 0.7965, R^2 = 0.9017 \quad (3)$$

One can calculate the order of the non-linear process, *q*, and the constant, *c*, as follows:

$$\frac{1}{q} = 0.2996 \text{ -> } q \approx 3 \quad (4)$$

$$ln(c) = 0.7965 \text{ -> } c \approx 1 \quad (5)$$

The higher the order of the non-linearity, the flatter is the slope of the line.

Figure 5. Writing fields varying the laser power at seven different scanning speeds for a sweep of the interface between substrate and photoresist in use (0,5um, 0.8um and 1,0um). We can trigger when the polymerization starts, check the materials response and observe the damage threshold.

Hence, in the cases of the other two tested photoresists, the order of non-linear process is ≈ 3 and ≈ 3.5, respectively. It has been suggested that multi-photon photoionization and possibly subsequent avalanche ionization could be the dominating absorption/initiation mechanism in 3D DLW [17]. In this study, we do not try to gain any chemical insight into the processes involved, and restrict us to a quantitative study of a multi-photon process. We will discuss this polymerization threshold model in detail elsewhere.

For the experimental verification, we wrote lines of 10um varying the laser power at seven different scanning speeds; the scanning speed was varying two-fold (from 1.6 um/sec to 102um/sec) and laser power started at 1 mW, increasing in

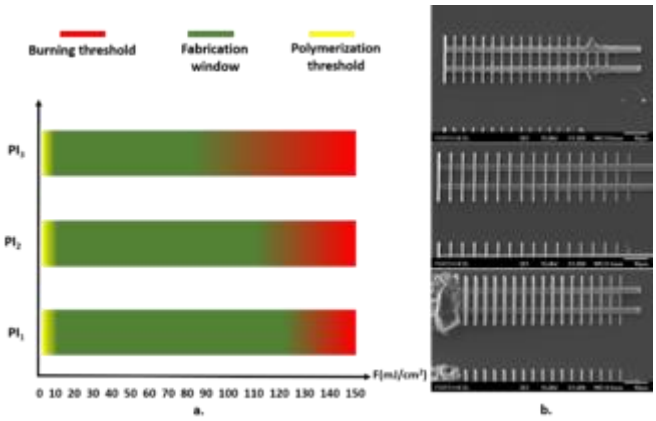

steps of 1 mW, up to 15 mW. The fabricated lines can be evaluated *in situ*. Thus, one can follow the process and can check how much power is needed at a specific scanning speed. The laser beam needs to be focused at the interface between the glass substrate and the photoresist in use. This is done by moving the sample closer to the focusing lens, while observing from the CCD. When polymerization becomes visible, the laser beam is focused inside the photoresist. Ideally, the laser beam is focused barely inside the photoresist. That way, the base of the structure is fabricated at the interface and is attached on the glass substrate. If the interface is overestimated, the structure will not attach on the glass substrate and will be lost inside the photoresist. On the other hand, if the interface is underestimated, part of the structure will be built inside the glass substrate. By washing out with organic solvents the non-polymerized material, we observe the 3D structure. Once the lines are fabricated, the sample can be evaluated by SEM (Figure 5).

3.2 Process window

Just listing scanning speed as the main throughput defining parameter is insufficient, as it does not specify the size of formed features. Therefore, we produced resolution bridges, where suspended lines (80 um long) were structured with different fluences from 10 mJ/cm^2 to 150 mJ/cm^2. The average

laser power was measured before the microscope objective, so after its loses only 20% of the incident laser power reaches the sample. This condition is applied for every structure. Each suspended line was written using a single laser pass. The obtained resolution bridges were analyzed by scanning electron microscopy (SEM). The quality of the suspended lines was evaluated using a three-colour classification: class A (yellow) defines the polymerization threshold and class B (green) fine lines. Lines rated as class C (red) have burst regions (Figure 6).

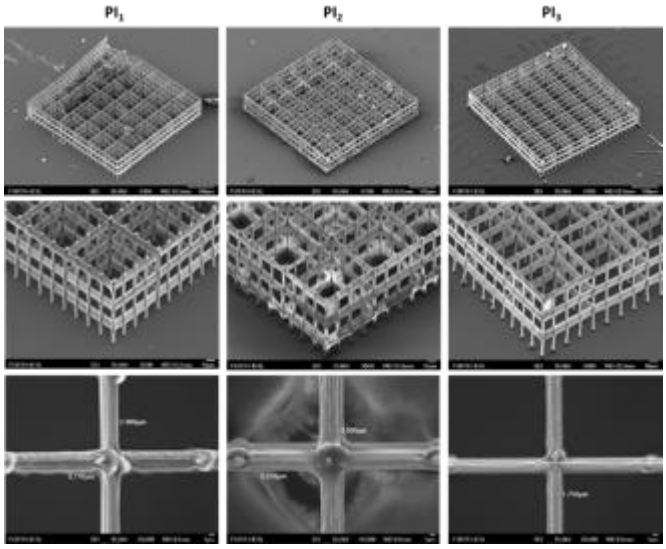

Figure 6. Process window. **a.** *Polymerization threshold is defined as the lowest fluence that yields well defined lines after the development process and burning threshold when bubble formation and material damage starts.* **b.** *SEM images of the fabricated resolution bridges.*

3.3 Fabrication of 3D microstructures

A woodpile is a 3D structure of layers of one-dimensional rods with a stacking sequence that repeats itself every four layers. Generally, woodpiles have a face-centered-tetragonal (fct) lattice symmetry and can be used as resolution test in MPP.

All woodpiles were fabricated with scanning speed at 100μm/sec and laser fluence for PI_1, PI_2 and PI_3 was 72.02 mJ/cm^2, 82.30 mJ/cm^2 and 102.88 mJ/cm^2, respectively. After the polymerization process, the sample is being developed in solvent baths. First, the sample is immersed in a 50:50 solution of 1-propanol and 4-methyl-2-pentanone for 30min. Then, the sample is placed in 1-propanol for 15min, with an intermediate step of drying with N2 gas. These development steps serve to clean the surface from non-polymerized material. The following Figure 7 presents the fabricated woodpiles that show low shrinkage and a resolution of ~250 nm, ~373 nm and ~478 nm for PI_1, PI_2 and PI_3, respectively. The top surface's roughness, due to the organic solvent baths during development process, is depicted at the magnified top view of the fabricated woodpiles.

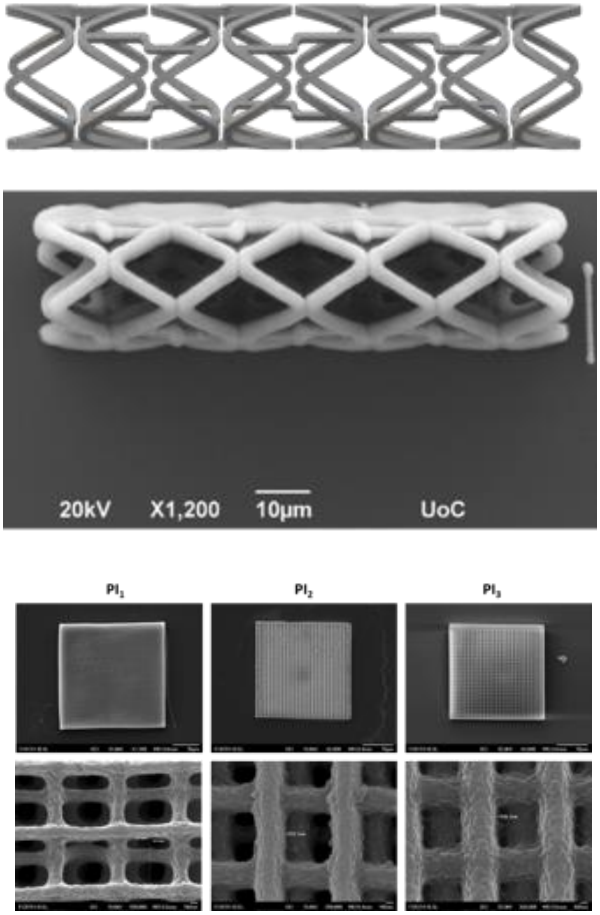

Figure 7. SEM images of woodpiles fabricated using the different photoinitiators discussed in this study and their magnified top view, respectively.

To highlight the versatility of these three benzaldehyde moieties as a new substance class of multi-photon lithography photoinitiators, next we have fabricated 3D designs with potential applications in biomimetics, 3D scaffolding and microfluidics.

An ideal micro-scaffold much have optimal pore size permitting effective cell seeding and strong material properties [18]. In this study, we fabricated 3D-microstructures (480×480×60μm^3) with porous size of 40um via MPL using an objective lens with 40x magnification. The scanning speed was 100um/sec and laser fluence was the same for PI_1 and PI_2, i.e. 113.69 mJ/cm^2 and 123.17 mJ/cm^2 for PI_3 (Figure 8). There is close matching between the experimental structure and the CAD model, since the unit cells are consistent and well-defined.

Figure 8. SEM images of micro-scaffolds fabricated by MPP. First row presents tilted view of the whole micro-scaffold for each photoinitiator in use. Second row presents zoomed photo of the one edge of the micro-scaffold and details of the unit cell connection are depicted in the third row.

Figure 9. 3D cylindric stent-like microstructure. **a.** Side view of the *CAD design.* **b.** *Top view of the SEM image of the fabricated microstructure by MPP.*

3.4 Biocompatibility tests

4. Conclusions

We need to discuss further the results and mention here the highlights!

Acknowledgements

The authors would like to acknowledge Prof. Athina Bakopoulou (School of Dentistry, Aristotle Univerasity of Thessaloniki) for generously providing the dental pulp stem cells under the approved protocol by the Institutional Ethics Committee (322/15-04-2013) and Mrs. Aleka Manousaki for SEM technical support. Aix Marseille University and The Centre National de la Recherche (CNRS) are acknowledged for financial supports. This research was also funded by the Agence Nationale de la Recherche (ANR agency) through the PhD grant of Guillaume Noirbent (ANR-17-CE08-0054 VISICAT project).

Conflict of Interest

The authors declare no coflict of interest.

References

[1] Kawata S., Sun H.-B., Tanaka T. and Takada K. 2001 *Nature* **412** 697
[2] Maruo S. and Fourkas J. 2008 *Laser Photon. Rev.* **2** 100
[3] Ɒinca V., Kasotakis E., Catherine J., Mourka A., Ranella A., Ovsianikov A., Chichkov B.N., Farsari M., Mitraki A. and Fotakis C. 2008 *Nanoletters* **8** 538-543
[4] Gansel K., Thiel M., Rill M. S., Decker M., Bade K., Saile V., von Freymann G., Linden S. and Wegener M. 2009 *Science* **325** 1513
[5] Camposeo A., Persano L., Farsari M. and Pisignano D. 2019 *Adv. Optical Mater.* **7** 1800419
[6] Narayan R. J., Doraiswamy A., Chrisey D. B. and Chichkov B. N. 2010 *Materiasl Today* **13** 12
[7] Goeppert-Mayer M. 1931 *Annalen der Physics (Leipzig)* **9** 273
[8] Farsari M. and Chichkov B. N. 2009 *Nat. Photonics* **3** 450-452
[9] Zhou X., Hou Y. and Lin J. 2015 *AIP Advances* **5** 030701
[10] Cumpston B. H., Sundaravel A. P., Barlow S., Dyer D. L., Ehrlich J. E., Erskine L. L., Heikal A. A., Kuebler S. M., Lee S. I.-Y., McCord-Maughon D., Qin J., Rockel H., Rumi M., Wu X.-L., Marder S. R., Perry J. W. 1999 *Nature* **398** 51-54
[11] Warther D., Gug S., Specht A., Bolze F., Nicoud J.-F., Mourot A. and Goeldner M. 2010 *Bioorg. Med. Chem.* **18** 7753-7758
[12] Li Z., Pucher N., Cicha K., Torgersen J., Ligon S. C., Ajami A., Husinsky W., Rosspeintner A., Vauthey E., Naumov S., Scherzer T., Stampfl J. and Liska R. 2013 *Macromolecules* **46** 352-361
[13] Ovsianikov A., Viertl J., Chichkov B., Oubaha M., MacCraith B., Sakellari I., Giakoumaki A., Gray D., Vamvakaki M., Farsari M. and Fotakis C. 2008 *ACS Nano* **2** 2257-2262
[14] Ligon S. C., Liska R., Stampfl J., Gurr M. and Mulhaupt R. 2017 *Chem. Rev.* **117** 10212-10290
[15] Mueller P., Thiel M. and Wegener M. A 2014 *Opt. Lett.* **39** 24
[16] Fischer J., Mueller J. B., Kaschke J., Wolf T. J., Unterreiner A.-N. and Wegener M. 2013 *Opti. Express* **21** 26244
[17] Mueller J. B., Fischer J., Mayer F., Kadic M. and Wegener M. 2014 *Adv. Mat.* **26** 6566
[18] Flamourakis G., Spanos I., Vangelaots Z., Manganas P., Papadimitriou L., Grigoropoulos C., Ranella A. and Farsari M. 2020 *Macromol. Mater. Eng.* 2000238